

Article

Effects of Notches and Defects on Dwell Fatigue Mechanism and Fatigue Life of Ti-6Al-4V ELI Alloy Used in Deep-Sea Submersibles

Jian Sun ^{1,2}, Lei Wu ^{3,*} and Chengqi Sun ^{1,2,*} 

¹ State Key Laboratory of Nonlinear Mechanics, Institute of Mechanics, Chinese Academy of Sciences, Beijing 100190, China; sunjian201@mails.ucas.ac.cn

² School of Engineering Science, University of Chinese Academy of Sciences, Beijing 100049, China

³ Guobiao (Beijing) Testing & Certification Co., Ltd., Beijing 101400, China

* Correspondence: wulei@gbtcgroup.com (L.W.); scq@lnm.imech.ac.cn (C.S.)

Abstract: The notch (i.e., stress concentration) and defect are important factors influencing the conventional fatigue behavior of metallic materials. What is the influence of notches and defects on the dwell fatigue mechanism and fatigue life? In this paper, the effects of notches and defects on the dwell fatigue behavior of the Ti-6Al-4V ELI alloy used in deep-sea submersibles are investigated under the load control mode. It is shown that the dwell fatigue is insensitive to the defect size (190–438 μm) compared to the conventional fatigue. For notched specimens, they all present fatigue failure mode under dwell fatigue testing, and the dwell fatigue life is higher than that of the smooth specimen at the same local maximum stress. The dwell of the maximum stress has no influence on the fatigue life and failure mechanism for notched specimens. Moreover, the facet feature is observed in the crack initiation region for both the conventional and dwell fatigue of notched specimens. Electron backscatter diffraction observation indicates that the feature of the fine line markings on the facet in the image by scanning electron microscope is due to the steps on the fracture surface of the α grain.

Keywords: titanium alloy Ti-6Al-4V ELI; notch; defect; dwell fatigue life; failure mechanism



Citation: Sun, J.; Wu, L.; Sun, C. Effects of Notches and Defects on Dwell Fatigue Mechanism and Fatigue Life of Ti-6Al-4V ELI Alloy Used in Deep-Sea Submersibles. *J. Mar. Sci. Eng.* **2021**, *9*, 845. <https://doi.org/10.3390/jmse9080845>

Academic Editors: Dong-Sheng Jeng and José A. F. O. Correia

Received: 20 June 2021

Accepted: 3 August 2021

Published: 4 August 2021

Publisher's Note: MDPI stays neutral with regard to jurisdictional claims in published maps and institutional affiliations.



Copyright: © 2021 by the authors. Licensee MDPI, Basel, Switzerland. This article is an open access article distributed under the terms and conditions of the Creative Commons Attribution (CC BY) license (<https://creativecommons.org/licenses/by/4.0/>).

1. Introduction

The dwell fatigue (i.e., cold creep fatigue, which refers to the dwell loading effect at temperatures lower than 200 °C [1,2]) behavior of titanium alloys has drawn great attention due to some of the components in the field of aviation and deep-sea (e.g., fan discs of engines, pressure hull of deep-sea submersibles) subjected to dwell fatigue loadings during service [1–7]. For example, many results have shown that the dwell of the maximum stress could greatly reduce the fatigue life of titanium alloys [8–10] and the dwell fatigue of titanium alloys often presents the feature of cleavage or quasi-cleavage facets in the crack initiation region [1,11,12]. The results for the titanium alloy Ti-6Al-2Sn-2Zr-3Mo-X indicated that the rise and fall time significantly affects the dwell fatigue life, and the dwell fatigue life with the rise and fall time could be correlated by a linear relation in log–log scale [13]. For the dwell fatigue of Ti-6Al-4V ELI alloy, it has been shown that the stress ratio has great influence on the dwell fatigue life and dwell fatigue failure mode [14]. The dwell fatigue life increases with an increase in the stress ratio at the same maximum stress, and a specimen at a negative stress ratio tends to undergo ductile failure mode.

The actual component parts usually inevitably contain defects during the manufacturing process or from impacts of debris during service. They also might have a change in geometry (i.e., stress concentration) in order to meet the demands of design. These defects [15–18] and notches [19–22] play an important role in the conventional fatigue performance of metallic materials. For instance, the specimen of EA4T railway axles with artificial defects showed a lower fatigue strength than that of the smooth specimen [23].

The notch reduced the fatigue strength of the titanium alloy Ti-6Al-2Sn-2Zr-3Mo-X used for the pressure hull of deep-sea submersibles in terms of nominal stress [24]. However, there are few studies reported on the effects of notches and defects on dwell fatigue behavior. What is the influence of notches and defects on the dwell fatigue life and dwell fatigue mechanism? How does dwell loading affect the fatigue behavior of notched specimens and defective specimens? These are important issues for the safety evaluation of components subjected to dwell fatigue loading during service.

In this paper, the effects of notches and defects on dwell fatigue behavior were investigated for the Ti-6Al-4V ELI alloy used in deep-sea submersibles. The fatigue fracture surface was observed using a scanning electron microscope (SEM) and electron backscatter diffraction (EBSD) with the help of the focused ion beam (FIB) technique. The variation of cumulative maximum strain with the number of loading cycles was analyzed for the notched specimens under both conventional fatigue and dwell fatigue tests. The effect of defects on the dwell fatigue behavior was also compared with that of the conventional fatigue behavior. Moreover, the effects of dwell loading on the fatigue behavior of notched specimens and defective specimens are discussed.

2. Materials and Methods

2.1. Materials

The material used in this paper was a Ti-6Al-4V ELI alloy, which was cut from a forged then rolled plate, parallel to the rolling direction. The chemical composition is shown in Table 1. The average tensile stress was 879 MPa and the yield strength was 831 MPa, which were obtained from two specimens with a gauge length of 30 mm and diameter of 5 mm. The stress and strain curve is illustrated in Figure 1. The microstructure of the material perpendicular to the specimen axis consisted of approximately equiaxed α -phase and lamellar β_{tran} , as shown in Figure 2.

Table 1. Chemical composition (wt.%) of the Ti-6Al-4V ELI alloy.

Elements	Al	V	Fe	C	H	O	Ti
wt.%	6.45	4.08	0.19	0.0055	0.0033	0.11	balance

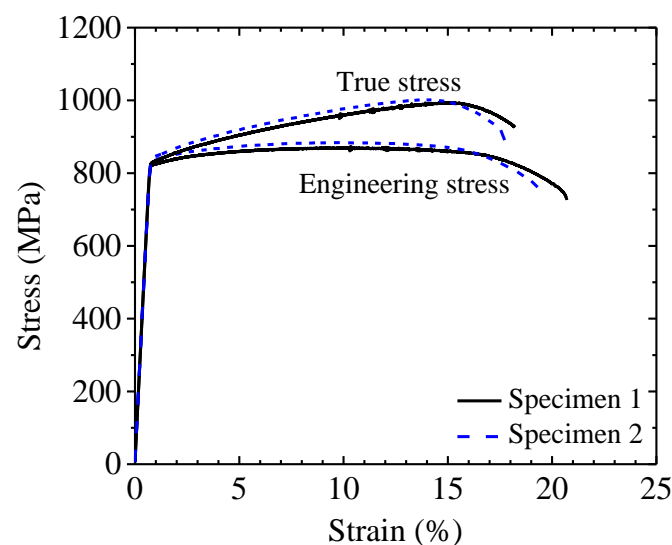


Figure 1. Stress and strain curve under tensile test.

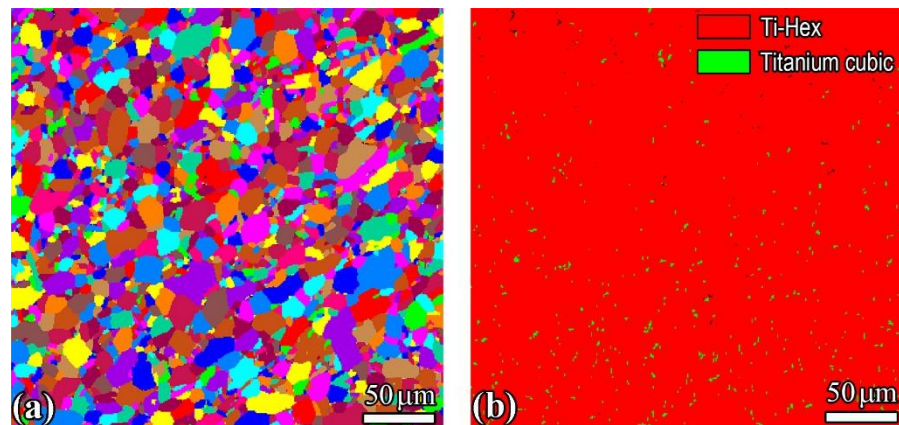


Figure 2. Microstructure of the Ti-6Al-4V ELI alloy. (a) EBSD grain map and (b) EBSD phase map corresponding to (a).

2.2. Test Methods

The dwell fatigue and conventional fatigue tests were performed in load control mode by an MTS Landmark machine in air and at room temperature. A continuous trapezoid wave was used for the dwell fatigue test, and a continuous triangular wave was used for the conventional fatigue test, as shown in Figure 3. The rise time and the fall time were 2 s for both the dwell fatigue and conventional fatigue tests. The stress ratio R was 0. The cumulative strain during the dwell fatigue and conventional fatigue tests was measured with an extensometer of 10 mm for notched specimens.

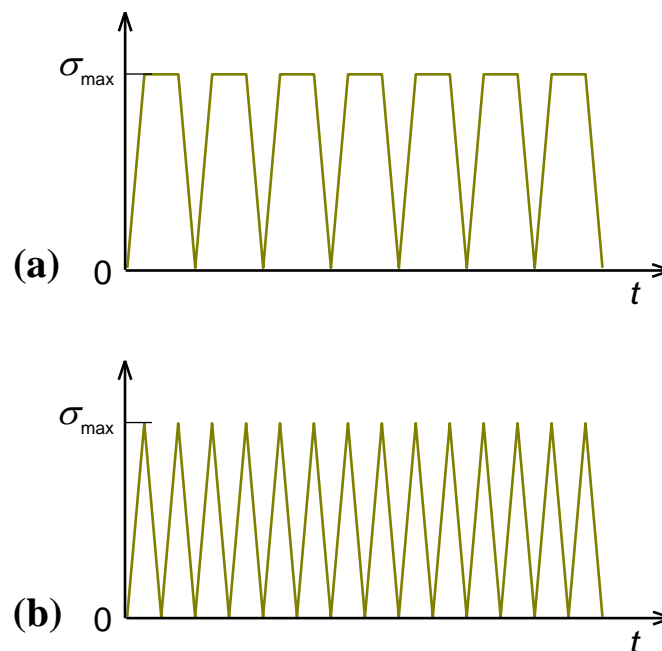


Figure 3. Schematics of loading waveforms. (a) Dwell fatigue loading; (b) Conventional fatigue loading.

Three types of specimens were used. One was a smooth specimen (Figure 4a), one was a notched specimen with a circumferential notch (Figure 4b), and the other was a defective specimen with one drilled hole in the middle of the gauge section of the smooth specimen in Figure 4a by a micro milling machine with different bit diameters (0.3, 0.8 and 1.8 mm) and associated depths (0.15, 0.2 and 0.25 mm). The elastic stress concentration factor for the notched specimen, which is defined as the ratio of the maximum principal stress at the notch root to that of the cylindrical specimen with the same minimum diameter as the

notched specimen under identical loading conditions, was 1.3. Before the fatigue tests, the surface of the gauge part of the smooth specimen and the notched part of the notched specimen were ground and polished. For the defective specimen, the defect was drilled after the surface of the gauge part of the smooth specimen was ground and polished.

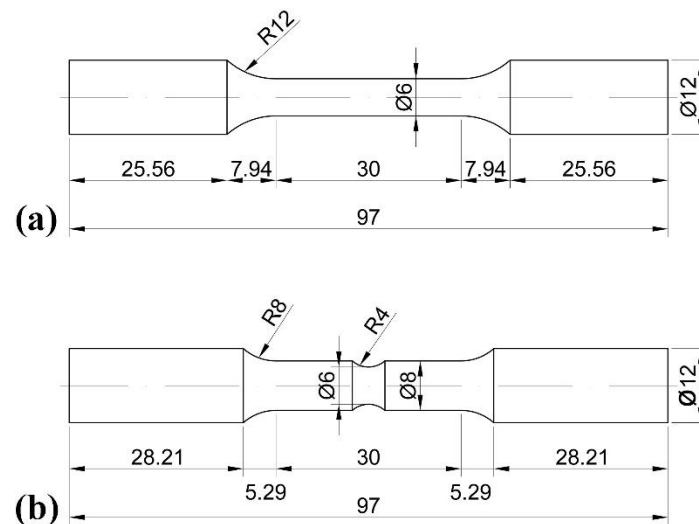


Figure 4. Shapes and dimensions of specimens under dwell fatigue and conventional fatigue tests (in mm). (a) Smooth specimen; (b) specimen with a circumferential notch.

2.3. Observation Methods

The fracture surface morphologies were observed by SEM for all the failed specimens. A cross-section sample parallel to the loading direction was prepared for the crack initiation region by employing FIB technique and then observed by EBSD on the Oxford Instruments. The fracture surface of the cross-section sample was protected by a thin coating layer of platinum during the cutting process by FIB technique.

3. Experimental Results and Analyses

3.1. Fatigue Performance of Tested Specimens

3.1.1. S-N Data of Notched Specimens

Figure 5 shows the S-N (i.e., stress-number of cycles to failure) data of the notched specimens under dwell fatigue and conventional fatigue tests. The results for the smooth specimen under conventional fatigue testing are also presented in Figure 5b. In Figure 5a, the nominal maximum stress was used, which is defined as the maximum stress of the cylindrical specimen with the same minimum diameter as the notched specimen under identical loading conditions. In Figure 5b, the local maximum stress (i.e., the local maximum principal stress) at the notch root was obtained by using the finite element analysis, and the stress and strain relation of specimen two in Figure 1 was used for the calculation. For the smooth specimen, the local maximum stress was taken as the nominal maximum stress.

It is seen in Figure 5 that, for the present notched specimens and the loading conditions, the dwell of the maximum stress had no influence on the fatigue life. This indicates that the effect of dwell loading on the notched specimen was very different from that on the smooth specimen when the dwell stress was in terms of the local stress. The dwell stress reduced the fatigue life of smooth specimens when the dwell maximum stress was near or greater than the yield strength for titanium alloys [10,11,14]. Furthermore, Figure 5b indicates that the dwell fatigue life of the notched specimen was higher than that of the smooth specimen at the same local maximum stress by the fact that the fatigue life decreased with the increase in the maximum stress at the same stress ratio and the dwell fatigue life was no more than the conventional fatigue life for the maximum stress dwell [10,11,14].

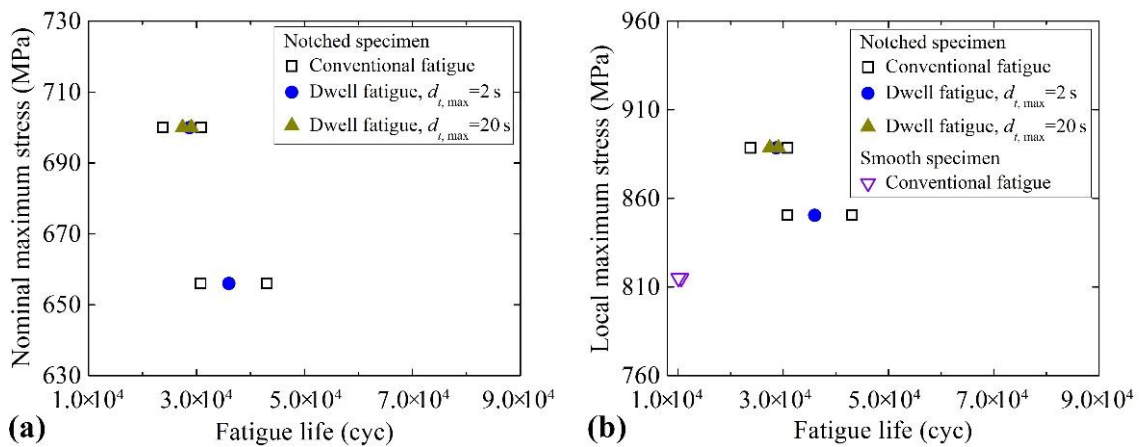


Figure 5. Comparison of fatigue performance between dwell fatigue test and conventional fatigue test for notched specimens. (a) Nominal maximum stress and fatigue life; (b) local maximum stress and fatigue life, which is also compared with the conventional fatigue life of the smooth specimen.

3.1.2. Fatigue Life Data of Defective Specimens

Figure 6 shows the variation of the fatigue life with the defect size of the defective specimens under dwell fatigue and conventional fatigue testing. In Figure 6, the nominal maximum stress for the defective specimen is defined as the nominal maximum stress of the smooth specimen under identical loading conditions, i.e., the defect was not considered for the calculation of the nominal maximum stress. The defect size was taken as the square root of the projection area of the defect perpendicular to the principal stress direction [25], and was measured from the SEM image of the fracture surface for the defect induced failure or the cross-section of the specimen not failed from the defect by the Image-Pro Plus software. It is seen in Figure 6 that the defect had an influence on the fatigue life under conventional fatigue testing. The specimen with the bigger defect showed a lower fatigue life, similar to that for the effect of surface artificial defects on the fatigue life of steels [26–28]. While the dwell fatigue life is independent of the defect size. In fact, all the defective specimens did not fail from the defect under dwell fatigue testing in comparison with those that the fatigue crack initiated from the defect for all the defective specimens under conventional fatigue testing. This indicates that the dwell fatigue is not sensitive to the defect compared to conventional fatigue. Figure 6 also indicates that the dwell of the maximum stress reduced the fatigue life of the defective specimen.

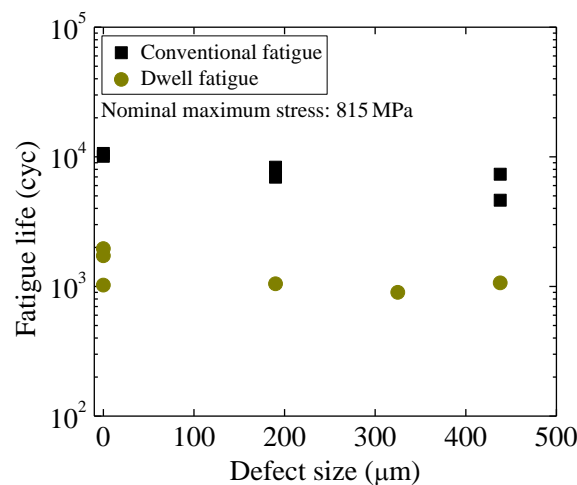


Figure 6. Comparison of fatigue performance between dwell fatigue test and conventional fatigue test for defective specimens.

3.2. Fatigue Fracture Surface Observation

3.2.1. Smooth Specimens and Defective Specimens under Conventional Fatigue Testing

SEM observation indicated that the smooth specimens all failed from the specimen surface and the fracture surface exhibited multiple crack initiation sites under conventional fatigue testing. The defective specimens all failed from the defect under conventional fatigue testing. Figure 7 shows the morphologies of the fracture surface of several smooth specimens and defective specimens under conventional fatigue testing. Furthermore, it is observed that there is a facet feature in the crack initiation region for the smooth specimen (Figure 7b,c) and in the vicinity of the defect for the defective specimen (Figure 7f,i), similar to that observed in the Ti-6Al-4V alloy [29,30].

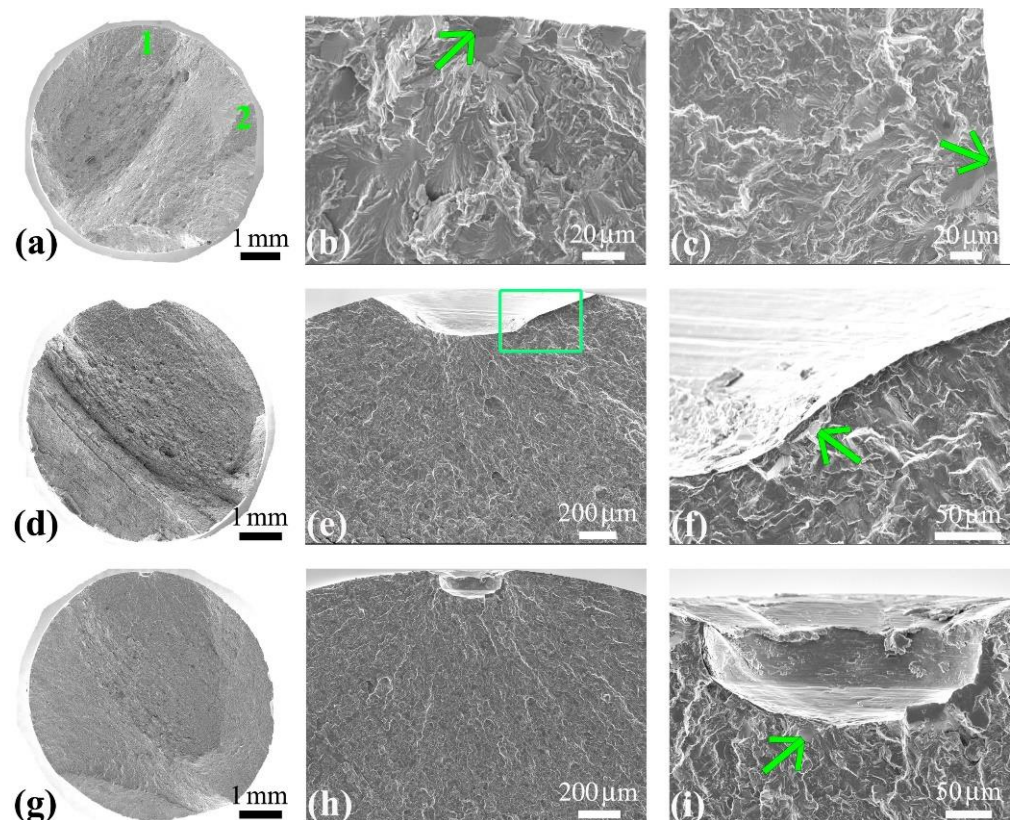


Figure 7. Morphologies of fracture surface of several failed specimens at $\sigma_{\max} = 815$ MPa under conventional fatigue testing. (a–c): Smooth specimen with $N_f = 10,623$ cycles, (b,c) are magnified images of crack initiation regions 1 and 2 in (a), respectively; (d–f): defective specimen with $N_f = 4621$ cycles, (e,f) are magnified images of crack initiation region in (d) and the rectangular region in (e), respectively; (g–i): defective specimen with $N_f = 6961$ cycles, (h,i) are magnified images of crack initiation regions in (g,h), respectively. The arrows point to the small regions exhibiting facet feature.

3.2.2. Smooth Specimens and Defective Specimens under Dwell Fatigue Test

It has been shown that the fracture surface of dwell fatigue of the Ti-6Al-4V ELI alloy exhibited three types of failure mode [14]: fatigue failure mode, ductile failure mode and mixed failure mode. The smooth and defective specimens all exhibited fatigue crack initiation and growth in some local regions in the fracture surface (Figure 8b,d), but the fracture was due to both the fatigue crack and the plastic deformation, i.e., the smooth and defective specimens presented the mixed failure mode [14]. It is noted that the defective specimens did not all fail from the defect under dwell fatigue testing in this paper.

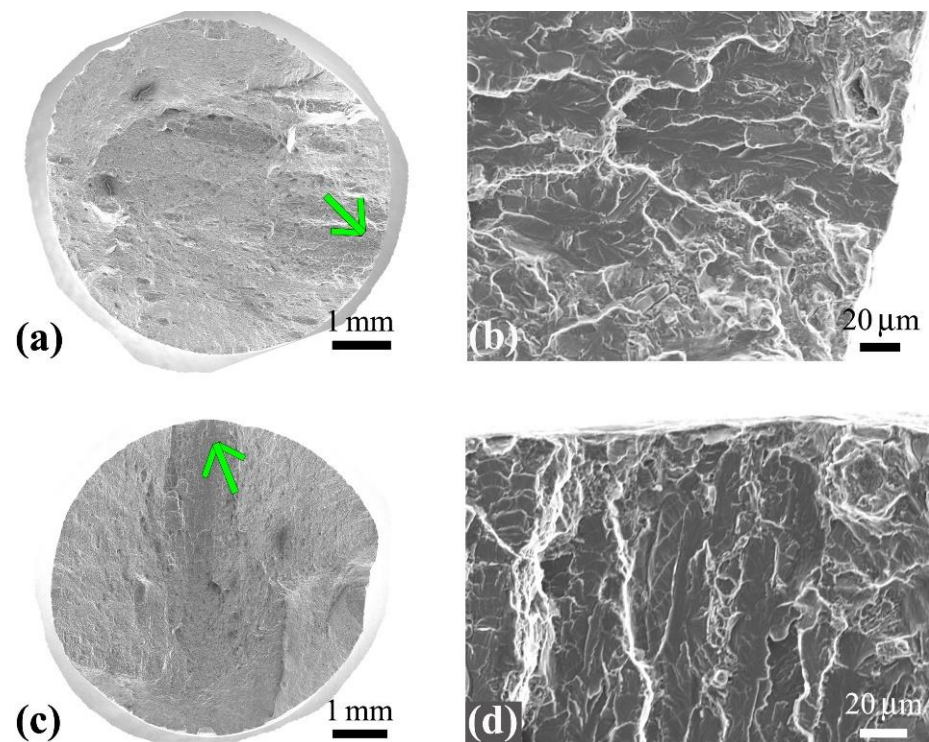


Figure 8. Morphologies of fracture surface of failed specimens at $\sigma_{\max} = 815$ MPa and $d_{i,\max} = 120$ s under dwell fatigue testing. (a,b): Smooth specimen with $N_f = 1724$ cycles; (c,d): Defective specimen with $N_f = 1066$ cycles. (b,d) are magnified images of the regions where the arrows point to in (a,c), respectively.

3.2.3. Notched Specimens under Conventional and Dwell Fatigue Tests

SEM observation indicated that the notched specimens under conventional fatigue test all presented multiple crack initiation sites from the specimen surface (Figure 9a,d), and there was a facet feature in the crack initiation region (locations one and two in Figure 9e). For the notched specimens under dwell fatigue testing, they all presented fatigue failure mode. One specimen failed from the single crack initiation site from the specimen surface (Figure 9g), and the others failed from multiple crack initiation sites from the specimen surface (Figure 9j,m). The facet feature was also observed in the crack initiation region under dwell fatigue testing (locations one and two in Figure 9i).

The loading information, fatigue life and failure mode for all the tested specimens are summarized in Table 2, in which the nominal maximum stress and minimum stress are used.

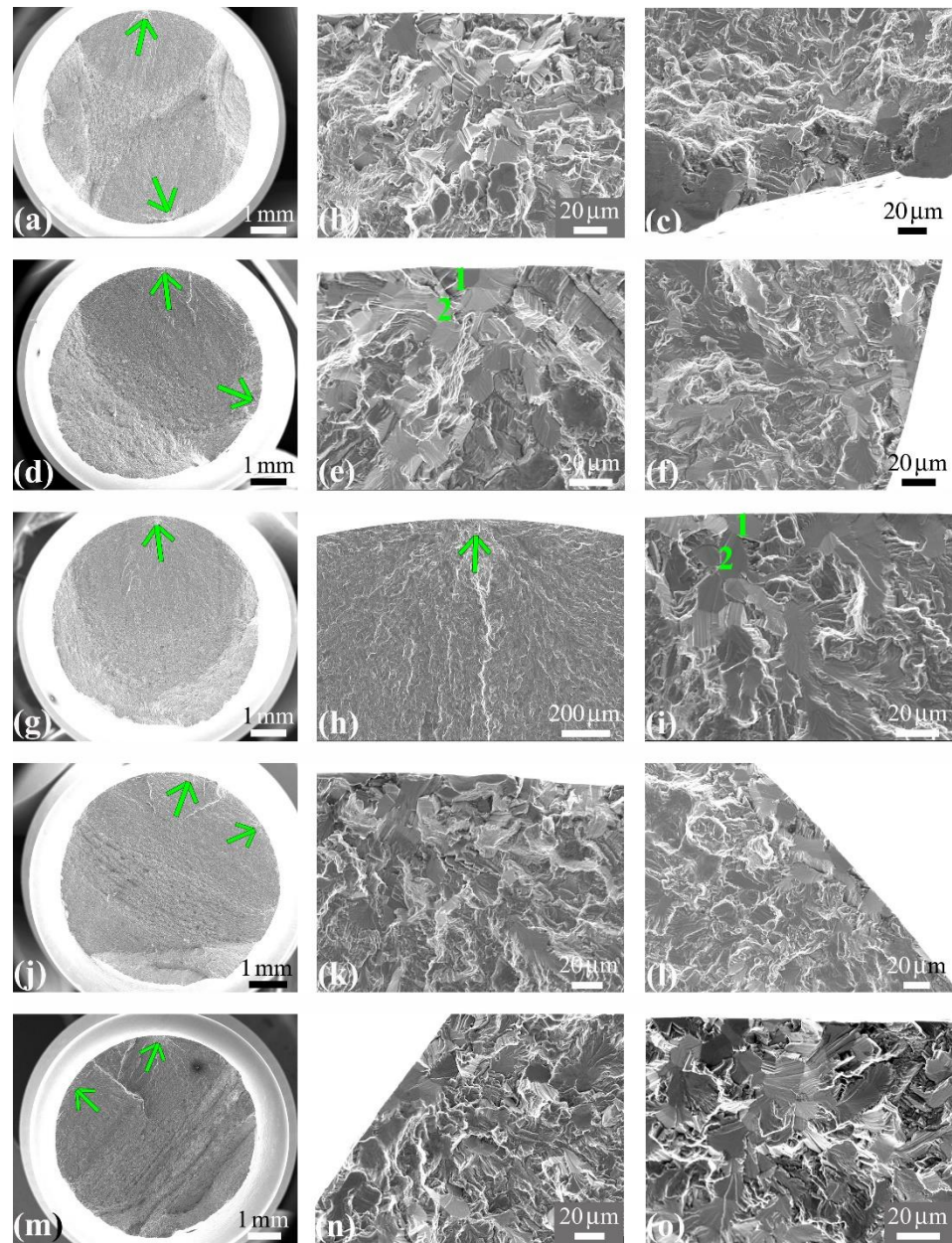


Figure 9. Morphologies of fracture surface of notched specimens. (a–c): conventional fatigue testing at nominal maximum stress $\sigma_{\max} = 656$ MPa and $N_f = 43,046$ cycles; (b,c) are magnified images of the regions where the up and down arrows point to in (a), respectively. (d–f): Conventional fatigue testing at nominal maximum stress $\sigma_{\max} = 700$ MPa and $N_f = 30,815$ cycles; (e,f) are magnified images of the regions where the up and right arrows point to in (d), respectively; The numbers 1 and 2 denote the locations exhibiting facet feature. (g–i): Dwell fatigue testing at nominal maximum stress $\sigma_{\max} = 656$ MPa, $d_{t,\max} = 2$ s and $N_f = 35,989$ cycles; (h,i) are magnified images of the regions that the arrow points to in (g,h), respectively; The numbers 1 and 2 denote the locations exhibiting facet feature. (j–l): Dwell fatigue test at nominal maximum stress $\sigma_{\max} = 700$ MPa, $d_{t,\max} = 2$ s and $N_f = 28,701$ cycles; (k,l) are magnified images of the regions where the top and right arrows point to in (j), respectively. (m–o): Dwell fatigue testing at nominal maximum stress $\sigma_{\max} = 700$ MPa, $d_{t,\max} = 20$ s and $N_f = 27,441$ cycles; (n,o) are magnified images of the regions where the left and up arrows point to in (m), respectively.

Table 2. Loading information, fatigue life and failure mode for the tested specimens.

Type of Specimen	Maximum Stress/MPa	Dwell Time $d_{t,max}/s$	Minimum Stress/MPa	Fatigue Life/cycle	Defect Size/ μm	Failure Mode
Smooth	815	0	0	10,623	-	Fatigue
Smooth	815	0	0	10,100	-	Fatigue
Smooth	815	120	0	1956	-	Mixed
Smooth	815	120	0	1724	-	Mixed
Smooth	815	120	0	1024	-	Mixed
Defective	815	0	0	7342	438	Fatigue
Defective	815	0	0	4621	438	Fatigue
Defective	815	0	0	8310	190	Fatigue
Defective	815	0	0	6961	190	Fatigue
Defective	815	120	0	1066	438	Mixed
Defective	815	120	0	900	325	Mixed
Defective	815	120	0	1049	190	Mixed
Notched	656	0	0	43,046	-	Fatigue
Notched	656	0	0	30,800	-	Fatigue
Notched	700	0	0	30,815	-	Fatigue
Notched	700	0	0	23,747	-	Fatigue
Notched	700	2	0	28,701	-	Fatigue
Notched	656	2	0	35,989	-	Fatigue
Notched	700	20	0	29,059	-	Fatigue
Notched	700	20	0	27,441	-	Fatigue

4. Discussion

4.1. Effect of Dwell Loading on Cumulative Strain for Notched Specimens

For smooth specimens of the Ti-6Al-4V ELI alloy [14], the dwell of the maximum stress increased the cumulative strain compared to the conventional fatigue at the same loading cycle. Here, the effect of dwell loading on the cumulative maximum strain for the notched specimen is presented in Figure 10. The fracture positions were all within the extensometer. It is seen from Figure 10 that the effect of the maximum stress dwell had no influence on the cumulative maximum strain at the initial loading cycles. For both the conventional fatigue and dwell fatigue tests, the cumulative maximum strain varied very little with the loading cycle within a certain number of loading cycles before the failure of the specimen. When the loading cycle tended to the fatigue life, the cumulative maximum strain increased or decreased with the increase in the loading cycle. It was found that this phenomenon was due to the position of the extensometer with respect to the fatigue crack for both the conventional fatigue and dwell fatigue tests. When the extensometer and the crack were on the same side, the cumulative maximum strain increased with an increase in the loading cycle. On the contrary, when the extensometer was on the back side of the crack, the cumulative maximum strain decreased with an increase in the loading cycle.

The finite element analysis was also employed for a further explanation of the results in Figure 10, in which a semi-elliptical shape crack with 0.2 mm thickness was considered [31]. The finite element model and the shape of the semi-elliptical crack are shown in Figure 11a,b, respectively. The tetrahedral elements were taken, and refinement meshes (0.1 mm in size) were used for the region around the crack. The tensile load of 18,539 N was applied at the two ends of the specimen, which corresponded to the nominal stress of 656 MPa at the notch root of the specimen. The stress and strain relation of specimen two in Figure 1 was used for calculation. Figure 11d shows the deformation distribution of the 10 mm part of the specimen containing the crack. It is seen that the deformation of the 10 mm part of the specimen containing the crack (i.e., the strain measured by the extensometer) was nonuniform, which is related to the position relative to the crack. For the crack region, the deformation was relatively big, while for no crack region, the deformation was relatively small. Figure 12 shows the variation of the strain of the 10 mm part containing the crack with the angle θ of the projection of the position of extensometer on the smallest plane relative to the center line of the crack shown in Figure 11b. It is seen that

the strain decreased when the angle of the position of extensometer relative to the center line of the crack increased from 0 to 180°. Figure 12 indicates that the cumulative strain measured at different position was different due to the nonuniform deformation caused by the existence of the crack. Figure 12 also indicates that the difference of the cumulative strain measured at a different position was related to the crack size. When the crack was very small, this difference was negligible.

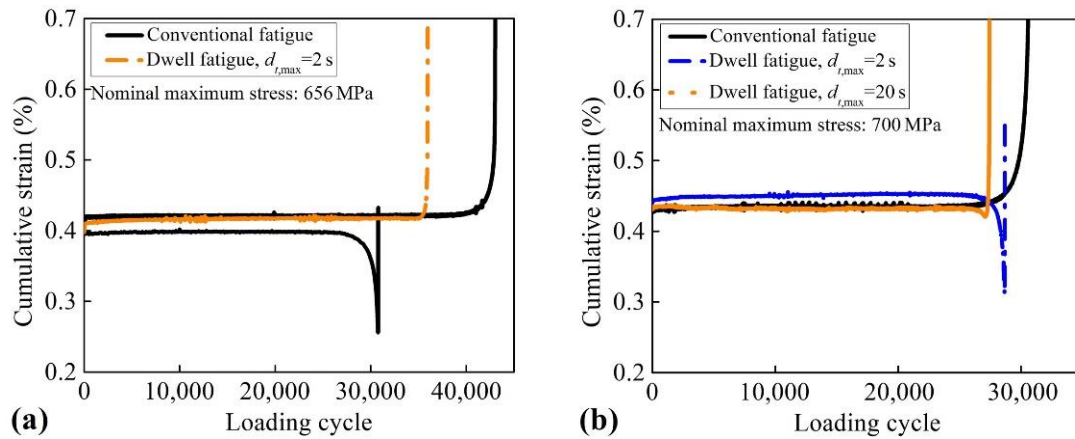


Figure 10. Variation in cumulative maximum strain with the number of loading cycles for notched specimens under conventional fatigue and dwell fatigue tests. (a): fatigue test at the nominal maximum stress $\sigma_{max} = 656$ MPa; (b): fatigue test at the nominal maximum stress $\sigma_{max} = 700$ MPa.

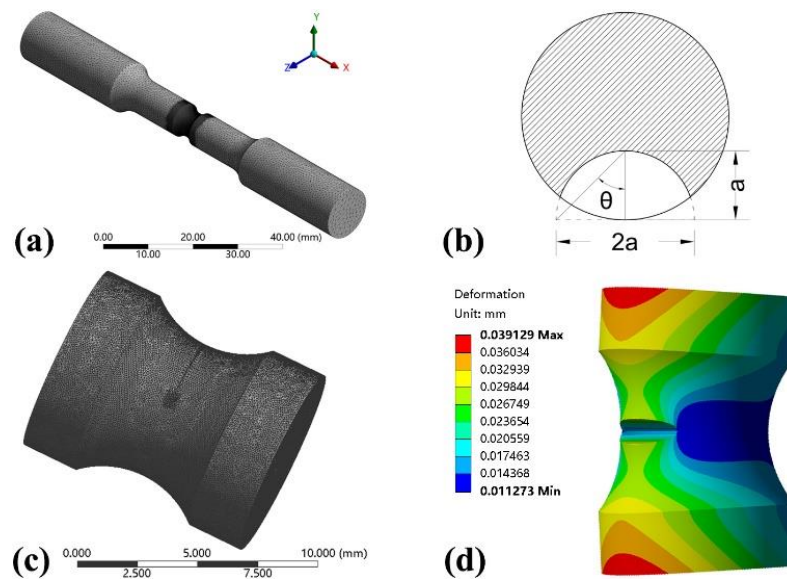


Figure 11. (a): Model of the specimen with the a crack in the plane of the smallest section of the specimen; (b): Sketch map of the semi-elliptical shape crack in (a); (c): Enlarged view of the 10 mm part containing the crack $a = 2.0$ mm in (a); (d): Deformation distribution of the 10 mm part in (c) under a tensile load of 18,539 N along the axis direction of the specimen.

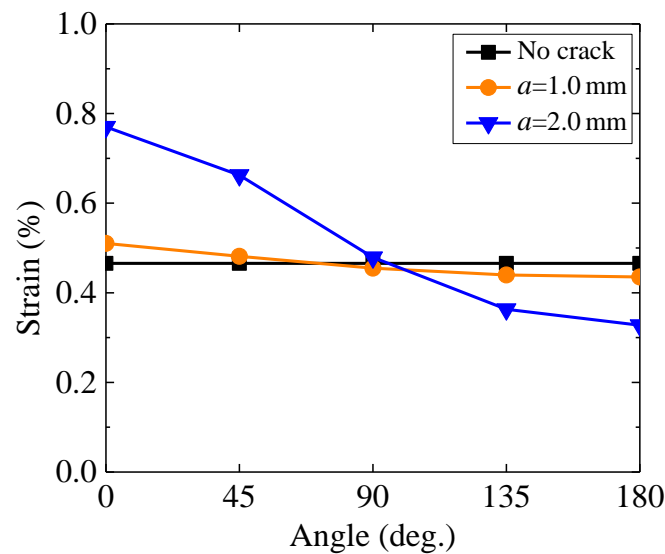


Figure 12. Variation of strain of the 10 mm part containing the crack with the angle θ of the projection of the position of extensometer on the smallest plane relative to the center line of the crack shown in Figure 11b.

Figure 10 also indicates that the effect of dwell loading on the cumulative strain was negligible for the notched specimen. This was different from the effect of dwell loading on the smooth specimen of the Ti-6Al-4V ELI alloy [14].

4.2. Effect of Dwell Loading on Fatigue Life of Notched Specimens

For the dwell fatigue of smooth specimens, the dwell loading increased the plastic strain accumulation and accelerated the damage in specimens, which resulted in a shorter fatigue life compared with the conventional fatigue [10,14]. While for the notched specimen, the cumulative plastic strain was not increased compared with the conventional fatigue for the present loading condition (Figure 10), indicating that the damage caused by the dwell loading could be negligible. This is consistent with the fracture surface observation of the notched specimens under dwell fatigue testing, in which all presented fatigue failure mode, i.e., the fatigue life was dominated by the crack initiation and growth. Therefore, the dwell of the maximum stress had negligible influence on the fatigue life.

4.3. Effect of Defect on Dwell Fatigue Life

The fatigue crack initiation was sensitive to the local defect, and the bigger defect usually resulted in a lower fatigue life [25–28]. For conventional fatigue of the present titanium alloy, the fatigue life was dominated by the crack initiation and growth caused by the defect, as shown in Figure 7d–i. So, the defect had an influence on the conventional fatigue life. While for the dwell fatigue, the fatigue life depended on not only the fatigue crack initiation and growth but also the plastic deformation due to the dwell loading [14]. In this case, the defect might not have been the main factor resulting in the failure of the specimen, as shown in Figure 8c,d. Therefore, the dwell fatigue was insensitive to the defect in comparison to the conventional fatigue.

4.4. Mechanism of Facet Formation

It has been shown in Figure 9 that there was a facet feature in the crack initiation region for notched specimens under both conventional fatigue and dwell fatigue testing. In fact, some facets were smooth (location one in Figure 9e,i) from the SEM observation, but the others were not smooth (location two in Figure 9e,i), which shows the feature of some fine linear markings on the facet. Here, the cross section of a facet with fine linear markings was observed by EBSD, as shown in Figure 13. It is seen that the facet was due to the fracture of the α grain and the fine line markings on the facet in SEM image

corresponded to the feature of the steps on the fracture surface of the α grain. According to the results in the literature, the facet could have been formed by a slip on the basal plane or prismatic planes of α grains [32,33], and it could also have formed due to the cleavage of α grains by dislocation pileups at grain boundaries or local high stress fields [33–35]. The kernel average misorientation (KAM) map is related to the geometrically necessary dislocations or accumulated plasticity [36,37]. The inverse pole figure map and the KAM map in Figure 13c,e indicate that the deformation was locally nonuniform for the α grain exhibiting the facet feature in Figure 13a due to the microstructure inhomogeneity and deformation incompatibility.

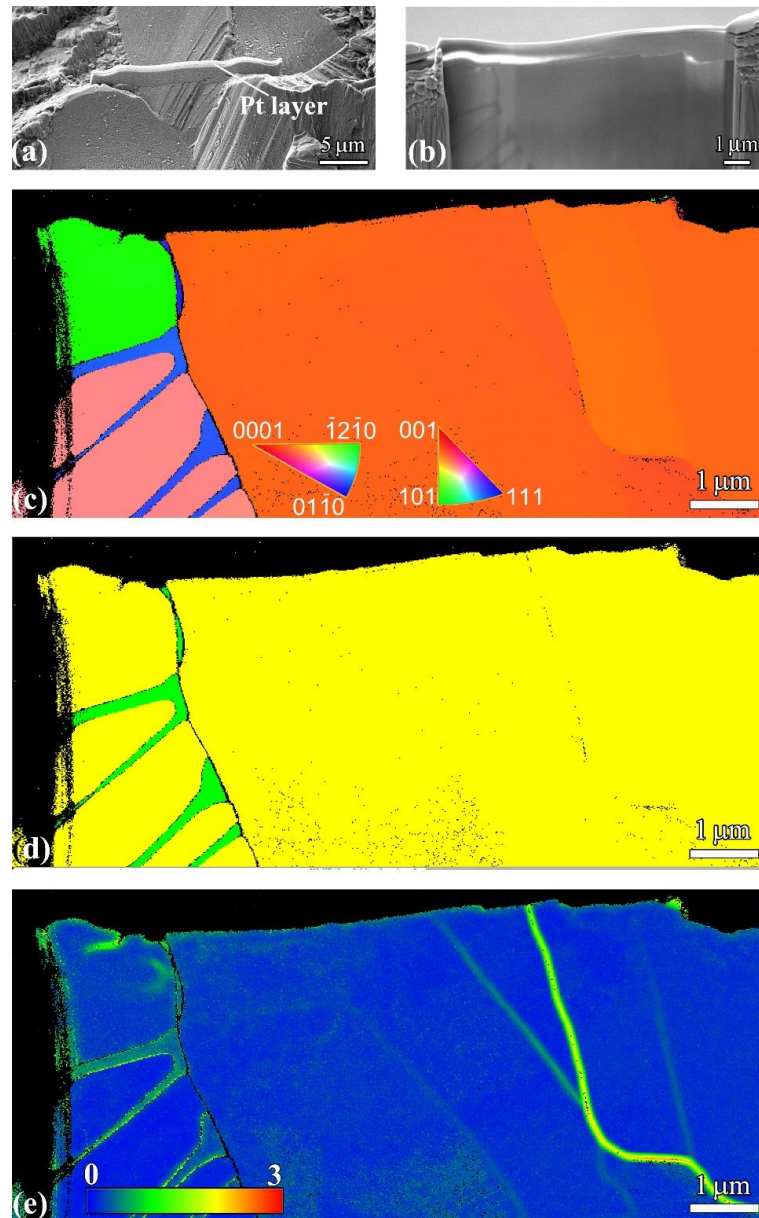


Figure 13. EBSD observation of extracted cross-section sample of the facet in location 2 in Figure 9i. (a): SEM image for FIB location; (b): SEM image of extracted cross-section sample; (c–e): EBSD results of the sample in (b), (c) is inverse pole figure map, (d) is phase map, in which the yellow and the green colors denote the alpha phase and the beta phase, respectively, (e) is the KAM map.

5. Conclusions

In this paper, we investigated the effects of notches and defects on the dwell fatigue behavior of the Ti-6Al-4V ELI alloy used in deep-sea submersibles. The main results are summarized as follows.

The notch had substantial influence on the dwell fatigue behavior of the Ti-6Al-4V ELI alloy. The dwell fatigue life of the notched specimen was higher than that of the smooth specimen at the same local maximum stress. The notched specimen presented fatigue failure mode under dwell fatigue testing. The dwell of the maximum stress had no influence on the fatigue life, failure mechanism and cumulative strain for the notched specimen of the Ti-6Al-4V ELI alloy.

The dwell fatigue behavior of the Ti-6Al-4V ELI alloy was insensitive to the defect size (190–438 μm). The defective specimen presented the mixed failure mode under dwell fatigue testing. The dwell of the maximum stress reduced the fatigue life of the defective specimen.

SEM and EBSD observations indicated that the facet in the crack initiation was due to the fracture of the α grain and the feature of the fine line markings on the facet in SEM image was attributed to the steps on the fracture surface of the α grain.

Author Contributions: Conceptualization, J.S., L.W. and C.S.; investigation, J.S., L.W. and C.S.; resources, L.W. and C.S.; visualization, J.S. and C.S.; writing—original draft preparation, J.S. and C.S.; writing—review and editing, J.S., L.W. and C.S.; supervision, C.S.; funding acquisition, C.S. All authors have read and agreed to the published version of the manuscript.

Funding: This research was funded by the National Natural Science Foundation of China Basic Science Center for “Multiscale Problems in Nonlinear Mechanics” (Grant No. 11988102) and the National Key Research and Development Program of China (Grant No. 2017YFC0305500).

Institutional Review Board Statement: Not applicable.

Informed Consent Statement: Not applicable.

Data Availability Statement: Not applicable.

Conflicts of Interest: The authors declare no conflict of interest.

References

1. Bache, M.R. A review of dwell sensitive fatigue in titanium alloys: The role of microstructure, texture and operating conditions. *Int. J. Fatigue* **2003**, *25*, 1079–1087. [[CrossRef](#)]
2. Qiu, J.K.; Ma, Y.J.; Lei, J.F.; Liu, Y.Y.; Huang, A.J.; Rugg, D.; Yang, R. A Comparative study on dwell fatigue of Ti-6Al-2Sn-4Zr-xMo ($x = 2$ to 6) alloys on a microstructure-normalized basis. *Metall. Mater. Trans. A* **2014**, *45*, 6075–6087. [[CrossRef](#)]
3. Waheed, S.; Zheng, Z.; Balint, D.S.; Dunne, F.P.E. Microstructural effects on strain rate and dwell sensitivity in dual-phase titanium alloys. *Acta Mater.* **2019**, *162*, 136–148. [[CrossRef](#)]
4. Li, Y.Z.; Bian, C.; Wang, K.; Sun, X.P.; Qin, C. Experimental study on dwell-fatigue of titanium alloy Ti-6Al-4V for offshore structures. *J. Ship Mech.* **2018**, *22*, 1124–1135.
5. Wang, F.; Jiang, Z.; Cui, W.C. Low-cycle dwell-fatigue life and failure mode of a candidate titanium alloy material TB19 for full-ocean-depth manned cabin. *J. Ship Mech.* **2018**, *22*, 727–735.
6. Zhang, Z.; Dunne, F.P.E. Phase morphology, variants and crystallography of alloy microstructures in cold dwell fatigue. *Int. J. Fatigue* **2018**, *113*, 324–334. [[CrossRef](#)]
7. Lavogiez, C.; Hémerly, S.; Villechaise, P. Analysis of deformation mechanisms operating under fatigue and dwell fatigue loadings in an α/β titanium alloy. *Int. J. Fatigue* **2020**, *131*, 105341. [[CrossRef](#)]
8. Evans, W.J.; Gostelow, C.R. The effect of hold time on the fatigue properties of a β -processed titanium alloy. *Metall. Trans. A* **1979**, *10*, 1837–1846. [[CrossRef](#)]
9. Bache, M.R.; Cope, M.; Davies, H.M.; Evans, W.J.; Harrison, G. Dwell sensitive fatigue in a near alpha titanium alloy at ambient temperature. *Int. J. Fatigue* **1997**, *19*, S83–S88. [[CrossRef](#)]
10. Wang, F.; Cui, W.C. Experimental investigation on dwell-fatigue property of Ti-6Al-4V ELI used in deep-sea manned cabin. *Mater. Sci. Eng. A* **2015**, *642*, 136–141. [[CrossRef](#)]
11. Evans, W.J. Time dependent effects in fatigue of titanium and nickel alloys. *Fatigue Fract. Eng. Mater. Struct.* **2004**, *27*, 543–557. [[CrossRef](#)]
12. Yang, L.N.; Liu, J.R.; Tan, J.; Chen, Z.; Wang, Q.; Yang, R. Dwell and normal cyclic fatigue behaviours of Ti60 Alloy. *J. Mater. Sci. Technol.* **2014**, *30*, 706–709. [[CrossRef](#)]

13. Song, Q.Y.; Li, Y.Q.; Wang, L.; Huang, R.X.; Sun, C.Q. Effect of rise and fall time on dwell fatigue behavior of a high strength titanium alloy. *Metals* **2019**, *9*, 914. [[CrossRef](#)]
14. Sun, C.Q.; Li, Y.Q.; Xu, K.L.; Xu, B.T. Effects of intermittent loading time and stress ratio on dwell fatigue behavior of titanium alloy Ti-6Al-4V ELI used in deep-sea submersibles. *J. Mater. Sci. Technol.* **2021**, *77*, 223–236. [[CrossRef](#)]
15. Jiang, Q.Q.; Sun, C.Q.; Liu, X.L.; Hong, Y.S. Very-high-cycle fatigue behavior of a structural steel with and without induced surface defects. *Int. J. Fatigue* **2016**, *93*, 352–362. [[CrossRef](#)]
16. Schonbauer, B.M.; Mayer, H. Effect of small defects on the fatigue strength of martensitic stainless steels. *Int. J. Fatigue* **2019**, *127*, 362–375. [[CrossRef](#)]
17. Kevinsanny; Okazaki, S.; Takakuwa, O.; Ogawa, Y.; Okita, K.; Funakoshi, Y.; Yamabe, J.; Matsuoka, S.; Matsunaga, H. Effect of defects on the fatigue limit of Ni-based superalloy 718 with different grain sizes. *Fatigue Fract. Eng. Mater. Struct.* **2019**, *42*, 1203–1213. [[CrossRef](#)]
18. Hu, Y.N.; Wu, S.C.; Withers, P.J.; Zhang, J.; Bao, H.Y.X.; Fu, Y.N.; Kang, G.Z. The effect of manufacturing defects on the fatigue life of selective laser melted Ti-6Al-4V structures. *Mater. Des.* **2020**, *192*, 108708. [[CrossRef](#)]
19. Haritos, G.K.; Nicholas, T.; Lanning, D.B. Notch size effects in HCF behavior of Ti-6Al-4V. *Int. J. Fatigue* **1999**, *21*, 643–652. [[CrossRef](#)]
20. Wang, J.K.; Yang, X.G. HCF strength estimation of notched Ti-6Al-4V specimens considering the critical distance size effect. *Int. J. Fatigue* **2012**, *40*, 97–104. [[CrossRef](#)]
21. Li, C.M.; Hu, Z.; Sun, C.Q.; Song, Q.Y.; Zhang, W.H. Probabilistic control volume method for evaluating the effects of notch size and loading type on fatigue life. *Acta Mech. Solida Sin.* **2020**, *33*, 141–149. [[CrossRef](#)]
22. Li, Y.B.; Song, Q.Y.; Yang, K.; Chen, Y.P.; Sun, C.Q.; Hong, Y.S. Probabilistic control volume method for the size effect of specimen fatigue performance. *J. Theor. App. Mech-Pol.* **2019**, *51*, 1363–1371. (In Chinese)
23. Gao, J.W.; Dai, G.Z.; Li, Q.Z.; Zhang, M.N.; Zhu, S.P.; Correia, J.A.F.O.; Lesiuk, G.; De Jesus, A.M.P. Fatigue assessment of EA4T railway axles under artificial surface damage. *Int. J. Fatigue* **2021**, *146*, 106157. [[CrossRef](#)]
24. Sun, C.Q.; Song, Q.Y. A method for predicting the effects of specimen geometry and loading condition on fatigue strength. *Metals* **2018**, *8*, 811. [[CrossRef](#)]
25. Murakami, Y. *Metal Fatigue: Effects of Small Defects and Nonmetallic Inclusions*; Academic Press: Oxford, UK, 2002.
26. Lei, Z.; Zhao, A.; Xie, J.; Sun, C.; Hong, Y. Very high cycle fatigue for GCr15 steel with smooth and hole-defect specimens. *Theor Appl. Mech. Lett.* **2012**, *2*, 031003. [[CrossRef](#)]
27. Zhang, J.; Li, H.; Yang, B.; Wu, B.; Zhu, S. Fatigue properties and fatigue strength evaluation of railway axle steel: Effect of micro-shot peening and artificial defect. *Int. J. Fatigue* **2020**, *132*, 105379. [[CrossRef](#)]
28. Akiniwa, Y.; Miyamoto, N.; Tsuru, H.; Tanaka, K. Notch effect on fatigue strength reduction of bearing steel in the very high cycle regime. *Int. J. Fatigue* **2006**, *28*, 1555–1565. [[CrossRef](#)]
29. Liu, X.L.; Sun, C.Q.; Hong, Y.S. Effects of stress ratio on high-cycle and very-high-cycle fatigue behavior of a Ti-6Al-4V alloy. *Mater. Sci. Eng. A* **2015**, *622*, 228–235. [[CrossRef](#)]
30. Nalla, R.K.; Boyce, B.L.; Campbell, J.P.; Peters, J.O.; Ritchie, R.O. Influence of microstructure on high-cycle fatigue of Ti-6Al-4V: Bimodal vs. lamellar structures. *Metall. Mater. Trans. A* **2002**, *33*, 899–918. [[CrossRef](#)]
31. Traupe, M.; Jenne, S.; Lütkepohl, K.; Varfolomeev, I. Experimental Validation of Inspection Intervals for Railway axles accompanying the engineering process. *Int. J. Fatigue* **2016**, *86*, 44–51. [[CrossRef](#)]
32. Szczepanski, C.J.; Jha, S.K.; Larsen, J.M.; Jones, J.W. Microstructural influences on very high cycle fatigue crack initiation in Ti-6246. *Metall. Mater. Trans. A* **2008**, *39*, 2841–2851. [[CrossRef](#)]
33. Everaerts, J.; Verlinden, B.; Wevers, M. Investigation of fatigue crack initiation facets in Ti-6Al-4V using focused ion beam milling and electron backscatter diffraction. *J. Microsc.* **2017**, *267*, 57–69. [[CrossRef](#)]
34. Sun, C.Q.; Li, Y.Q.; Huang, R.X.; Wang, L.; Liu, J.L.; Zhou, L.L.; Duan, G.H. Crack initiation mechanism and fatigue life of titanium alloy Ti-6Al-2Sn-2Zr-3Mo-X: Effects of stress ratio and loading frequency. *Mater. Sci. Eng. A* **2020**, *798*, 140265. [[CrossRef](#)]
35. Neal, D.F.; Blenkinsop, P.A. Internal fatigue origins in alpha-beta titanium-alloys. *Acta Metall.* **1976**, *24*, 59–63. [[CrossRef](#)]
36. Rui, S.S.; Shang, Y.B.; Su, Y.; Qiu, W.; Niu, L.S.; Shi, H.J.; Matsumoto, S.; Chuman, Y. EBSD analysis of cyclic load effect on final misorientation distribution of post-mortem low alloy steel: A new method for fatigue crack tip driving force prediction. *Int. J. Fatigue* **2018**, *113*, 264–276. [[CrossRef](#)]
37. Liu, X.L.; Xue, Q.Q.; Wang, W.; Zhou, L.L.; Jiang, P.; Ma, H.S.; Yuan, F.P.; Wei, Y.G.; Wu, X.L. Back-stress-induced strengthening and strain hardening in dual-phase steel. *Materialia* **2019**, *7*, 100376. [[CrossRef](#)]